



Cite this: *Nanoscale*, 2025, **17**, 26642

## Lithium aluminum titanium phosphate (LTP) composite solid-state electrolytes: progress and prospects for all-solid-state batteries

Yuyue Guo,<sup>†a</sup> Jiawei Zhao,<sup>†a</sup> Lingwang Liu,<sup>†a</sup> Xianshu Cai,<sup>a</sup> Hongliang Shi,<sup>b</sup> Fengrui Zhang,<sup>b</sup> Jingjing Xu<sup>\*c</sup> and Xiaodong Wu<sup>id</sup> <sup>\*a,b</sup>

Composite solid-state electrolytes (CSEs) based on lithium aluminum titanium phosphate (LTP) have become a pivotal research direction for next-generation solid-state lithium batteries (SSLBs), owing to their high ionic conductivity and excellent environmental stability. Despite the advantages conferred by its NASICON-type structure, LTP exhibits inherent brittleness and poor interfacial compatibility. By combining LTP with flexible polymers, CSEs effectively integrate the high ionic conductivity of the ceramic phase with the superior processability and interfacial adaptability of the polymer matrix. This review highlights key strategies for enhancing the performance of CSEs, including optimization of filler morphology and content, surface modification, incorporation of plasticizers/ionic liquids, and application of *in situ* polymerization techniques. Particular attention is given to critical challenges such as mitigating side reactions between LTP and lithium metal, suppressing lithium dendrite growth, and improving compatibility with high-voltage cathodes. Finally, we propose that future efforts should focus on interfacial engineering, scalable manufacturing, and computational modeling to facilitate practical implementation.

Received 10th August 2025,  
 Accepted 22nd October 2025

DOI: 10.1039/d5nr03393d

rsc.li/nanoscale

### 1. Introduction

With the growing global demand for high-energy-density and high-safety energy storage devices, conventional lithium-ion batteries (LIBs) employing organic liquid electrolytes face inherent limitations due to their safety risks, such as flammability, electrolyte leakage, and short circuits caused by lithium dendrite growth.<sup>1–3</sup> As an ideal candidate for next-generation battery technology, solid-state lithium batteries (SSLBs) replace liquid electrolytes with solid-state electrolytes, which are expected to fundamentally address safety concerns while providing a higher energy density and longer cycle life.<sup>4–6</sup> Solid-state electrolytes (SSEs) serve as the core component of solid-state batteries, with their performance directly determining the overall battery performance.

In the past few years, many different kinds of SSEs have been reported and these SSEs are primarily classified into three categories: inorganic solid-state electrolytes (ISEs), solid

polymer electrolytes (SPEs), and organic–inorganic composite solid-state electrolytes (CSEs).<sup>3–8</sup>

ISEs typically show high ionic conductivity along with excellent thermal stability, chemical stability, and mechanical strength. Common ISEs include oxides, sulfides, and halides.<sup>3</sup> Among these inorganic solid-state electrolytes, NASICON-structured compounds such as lithium aluminum titanium phosphate ( $\text{Li}_{1+x}\text{Al}_x\text{Ti}_{2-x}(\text{PO}_4)_3$ , abbreviated as LTP) and lithium aluminum germanium phosphate LAGP ( $\text{Li}_{1+x}\text{Al}_x\text{Ge}_{2-x}(\text{PO}_4)_3$ ) have been considered as among the most promising oxide-based inorganic solid-state electrolytes due to their high lithium-ion conductivity, excellent environmental stability, and relatively low cost. They have already achieved preliminary commercialization at a moderate scale.<sup>7,9–11</sup> However, there are still some defects including inherent inflexibility and brittleness, and easy reaction with the Li anode, which hinder their scalable manufacture and application in batteries.<sup>8,12–16</sup> The inherent brittleness makes it challenging to produce large-area, flexible thin films, while poor interfacial contact with rough electrode surfaces results in excessive interfacial impedance, a major obstacle for their application in all-solid-state batteries.<sup>17</sup> The poor electrochemical stability against lithium metal anodes makes them undergo side reactions that form high-resistance interphases or they even get reduced, leading to performance degradation and safety concerns.<sup>18</sup>

<sup>a</sup>*i-Lab, Suzhou Institute of Nano-Tech and Nano-Bionics, Chinese Academy of Sciences, Suzhou, Jiangsu 215123, China. E-mail: xdwu2011@sinano.ac.cn*

<sup>b</sup>*Tianmu Lake Institute of Advanced Energy Storage Technologies Co., Ltd, Liyang 213300, China*

<sup>c</sup>*College of Material Science and Engineering, Hohai University, Changzhou, Jiangsu 213200, China. E-mail: 20241052@hhu.edu.cn*

<sup>†</sup>These authors contributed equally to this work.



SPEs generally consist of polymer matrices and dissolved lithium salts, where segmental motion of polymer chains facilitates Li-ion transport. Polyethylene oxide (PEO) is the earliest and most extensively studied polymer matrix, valued for its ability to dissolve lithium salts and form flexible films. Other widely used polymers include polyvinylidene fluoride (PVDF), polyacrylonitrile (PAN), and polymethyl methacrylate (PMMA).<sup>19–21</sup> The main advantages of SPEs lie in their exceptional flexibility, processability, and favorable interfacial compatibility with electrodes, enabling accommodation of electrode volume changes and reduced interfacial resistance.<sup>7,8</sup> However, pure SPEs often suffer from low room-temperature ionic conductivity (significantly lower than inorganic or liquid electrolytes), insufficient mechanical strength to effectively suppress Li dendrite growth, and relatively narrow electrochemical windows, limiting their use in high-energy-density batteries.<sup>22–24</sup>

To overcome the drawback of single-component solid electrolytes, the development of organic–inorganic composite solid electrolytes (CSEs) by integrating inorganic oxide electrolytes with polymer electrolytes has emerged as a prominent research focus in solid-state batteries.<sup>5,12</sup> This composite strategy devotes to combine the high ionic conductivity and mechanical strength of inorganic fillers with the flexibility and interfacial compatibility of polymer matrices, thereby realizing solid electrolytes with superior comprehensive performance.<sup>10,14</sup>

This review systematically summarizes recent advances in LATP-based organic–inorganic composite electrolytes, including material fabrication, performance optimization, and battery applications. We critically analyze the merits and limitations of different composite strategies and provide perspectives on future research directions.

## 2. The research progress of LATP-based CSEs

LATP-based CSEs represent a critical research direction in this field, leveraging the high ionic conductivity of LATP to com-

pensate for the low conductivity of polymer matrices while utilizing polymer flexibility to address the processing challenges and interfacial issues inherent to LATP (Fig. 1).<sup>25</sup> Simultaneously, inorganic fillers can act as physical cross-linking points to enhance the mechanical strength of the polymer matrix and suppress lithium dendrite growth.<sup>26,27</sup> By carefully screening out the type, morphology, particle size, and loading of inorganic fillers, as well as adjusting the polymer matrix and interfacial structure, the overall performance of the CSEs can be significantly enhanced.

### 2.1 LATP-based CSEs with different polymer matrices

As we all know, the performance of CSEs is intrinsically linked to their composition (polymer matrix type, LATP content) and microstructure (filler morphology, dispersion state). Selecting an appropriate polymer matrix is fundamental for constructing high-performance LATP composite electrolytes.<sup>28</sup>

In 1975, Wright *et al.* revealed that PEO with alkali metal salts possesses ionic conductivity.<sup>29</sup> This discovery has set a precedent for the development of ion-conducting polymers. PEO has been extensively investigated because of its excellent lithium salt solvation capability and chain flexibility. When compounded with LATP, PEO-based electrolytes demonstrate enhanced ionic conductivity and mechanical properties.<sup>25,30</sup> However, the crystalline domains in PEO at room temperature can impede ion transport, necessitating the incorporation of LATP fillers or other additives to suppress crystallinity and increase amorphous regions, thereby improving the room-temperature conductivity.

PVDF and its copolymers (*e.g.*, PVDF-HFP) are also widely adopted as polymer matrices owing to their high dielectric constant and superior electrochemical stability.<sup>31</sup> However, PVDF faces similar challenges with PEO-based electrolytes at room temperature. To address this issue, researchers have proposed a “synergistic strategy”. This involves uniformly dispersing LATP particles within the polymer matrix to enhance its ionic conductivity. Simultaneously, the Lewis acid–base interactions between LATP and PVDF facilitate the dissociation of



Fig. 1 Schematic diagram of LATP<sup>10</sup> (Copyright 2014, ACS), LATP-polymer composite electrolyte, and the corresponding solid-state battery.



lithium salts, thereby increasing the concentration of free lithium ions. Thus, LAMP composites with these fluorinated polymers yield electrolyte membranes with balanced ionic conductivity and mechanical robustness.<sup>32</sup>

To explore composite polymer electrolytes with superior electrochemical properties and broader compatibility, researchers have developed a range of novel polymers, including polyacrylonitrile (PAN),<sup>33,34</sup> polyimide (PI),<sup>35</sup> poly(methyl methacrylate) (PMMA),<sup>36,37</sup> and poly(ethylene glycol) monomethacrylate (PEGMA).<sup>38</sup> Among these, PAN exhibits high ionic conductivity. The cyano groups (C≡N) in its molecular structure can interact with carbonyl groups (C=O) in the solvent, facilitating the formation of a stable electrode/electrolyte interphase. Studies have demonstrated that PAN-LAMP composite membranes prepared *via* electrospinning not only enhance the ionic conductivity, but also widen the electrochemical stability window.<sup>33,39</sup> However, due to the poor compatibility between the strong polar groups in PAN and lithium metal, severe electrode interface passivation occurs during prolonged cycling, exacerbating cell polarization and deteriorating the cycling stability.<sup>40</sup>

Simultaneously, PI exhibits unique advantages in safety applications due to its high thermal stability and flame retardancy. Leveraging these properties, He *et al.* designed a composite electrolyte membrane by coating a LAMP/PEO composite electrolyte onto an electrospun PI substrate. This membrane demonstrated thermal stability and self-extinguishing characteristics, maintaining structural integrity even at high temperatures (180 °C).<sup>41</sup> In contrast, PMMA, despite its excellent lithium salt dissociation capability and electrode compatibility, faces challenges such as strong viscoelasticity, difficulty in film formation, low ionic conductivity, and limited scalability for broader applications. To overcome the limitations of individual materials, researchers have designed hybrid polymer systems to harness their complementary advantages. For instance, the synergistic effect between the carbonyl groups of PMMA and the terminal hydroxyl groups of PEO chains facilitates the formation of a hydrogen bond network, enhancing mechanical strength and electrochemical stability.<sup>42,43</sup> Hybrid matrices incorporating LAMP fillers within PVDF-HFP/PEO blends achieved simultaneous improvements in ionic conductivity, tensile strength, and flexibility, while also exhibiting excellent compatibility with silicon anodes. Similarly, blending PAN with PEO yielded an electrolyte with enhanced flame retardancy and lower impedance.<sup>44</sup> This multi-phase design strategy effectively addresses the trade-offs between ionic transport and mechanical properties in single-polymer systems.<sup>45</sup> These systematic investigations into polymer matrix selection and modification provide critical guidelines for tailoring LAMP composite electrolytes to meet specific performance requirements in solid-state battery applications.

Innovative approaches also involve tailoring novel polymer structures. Trevisanello *et al.* investigated the impact of the polymer structure and crystallinity on the polymer-LAMP interfacial resistance, finding that the amorphous polymer-based electrolyte poly[2-(2-(2-methoxyethoxy)ethoxy)ethyl glycidyl

ether] (PTG) exhibited lower interfacial charge transfer resistance compared to PEO-based systems.<sup>46</sup>

In conclusion, the developed LAMP-based composite electrolytes effectively combine the advantages of both organic polymers and inorganic components. By adjusting the polymer molecular structure, improving preparation methods, and modifying the electrolyte interfaces, the ionic conductivity, mechanical robustness, and electrode interfacial stability can be effectively enhanced.<sup>37</sup> These experimental investigations offer valuable insights for developing next-generation high-performance all-solid-state lithium batteries with targeted functionalities.

## 2.2 LAMP-based CSEs with LAMP fillers of different contents and sizes

High-modulus LAMP fillers significantly reinforce polymer matrices, forming physical barriers against dendrite penetration. Simultaneously, homogeneous ion flux distribution and stable SEI formation are crucial.<sup>21</sup> The content of the LAMP filler significantly influences the performance of composite electrolytes. Typically, there exists an optimal filler content at which the composite electrolyte exhibits the highest ionic conductivity and the most superior overall performance. For instance, in PAN-LAMP composite electrolytes, studies have found that when the LAMP content reaches 20 wt%, the ionic conductivity and electrochemical stability of the electrolyte are enhanced.<sup>47</sup> In the PEO/LAMP system, a quasi-ceramic electrolyte containing 70 wt% LAMP and 30 wt% P(EO)<sub>15</sub>-LiTFSI also demonstrates relatively high conductivity at room temperature.<sup>30</sup> When the filler content is too low, the contribution of LAMP becomes negligible; conversely, excessive filler content may lead to particle agglomeration, increased interfacial impedance, and reduced flexibility of the polymer matrix, resulting in brittle and rigid composite films that are difficult to process and form poor interfacial contact with electrodes.<sup>48</sup>

In addition to the filler content, the morphology and size of the LAMP filler also play a critical role in determining the performance of composite electrolytes.<sup>27,49</sup> Compared to micron-sized particles, nano-sized LAMP particles possess a larger specific surface area, enabling the formation of more extensive interfacial regions with the polymer matrix. This facilitates the construction of additional ion transport pathways and may more effectively suppress polymer crystallization. For example, a sol-gel synthesized nano-sized LAMP filler has been shown to significantly enhance the ionic conductivity of composite electrolytes.<sup>50</sup> Although direct studies on LAMP nanofibers are limited in the provided literature, research on other NASICON-type materials or oxide nanofibers as fillers suggests that one-dimensional (1D) nanostructured fillers can form continuous network structures within the polymer matrix, providing rapid lithium-ion transport channels while improving the mechanical properties of composite electrolytes. This strategy of employing 1D-structured fillers also offers valuable insights for the design of LAMP-based composite electrolytes.<sup>51,52</sup> For example, Liu *et al.* reported a PEO-based composite electrolyte reinforced with an LAMP/PAN fiber network, forming a bicon-



tinuous structure that enhances mechanical properties while improving interfacial stability.<sup>45</sup>

### 2.3 Ion transport mechanisms

As shown in Fig. 2, the ion conduction in CSEs is a complex process compared to that in single-component systems, typically involving lithium-ion transport through the polymer phase, LAMP filler phase, and their interfacial regions.<sup>53,54</sup> Studies have demonstrated that the interfacial zones play a critical role in ion transport.<sup>55</sup> The interfacial zones between polymers and inorganic fillers may form space-charge layers or provide additional ion transport pathways due to interactions between polymer chains and filler surfaces, thereby improving the overall ionic conductivity.

The incorporation of inorganic fillers can disrupt the ordered arrangement of polymer chains, reduce crystallinity, and increase the proportion of amorphous regions, thereby enhancing the lithium-ion mobility within the polymer phase, particularly in PEO-based electrolytes.<sup>56</sup> These groups can promote the interaction with polymers and Li salts to the greatest extent, especially by greatly anchoring anions, weakening the affinity between Li ions and polymers, in order to accelerate the transport of Li ions and gain better compatibility at the filler–polymer interface.<sup>14</sup>

Simultaneously, the surface of inorganic fillers may interact with polymer chains or lithium salt anions, forming interfacial regions that facilitate lithium-ion dissociation and transport, a phenomenon often referred to as the “space-charge layer”

effect.<sup>55,57</sup> Furthermore, if the inorganic filler itself exhibits high ionic conductivity (e.g., LAMP), it can provide additional fast transport pathways for lithium ions, especially when the filler forms a percolating network within the polymer matrix.<sup>58</sup> For example, Zhu *et al.* proposed an innovative “polymer-in-ceramic” composite electrolyte strategy, where polymer-compatible ionic liquids (PCILs) were introduced to mediate interactions between the ceramic filler and polymer matrix. This approach established interpenetrating lithium-ion conduction channels, significantly improving both the ionic conductivity and lithium-ion transference number.<sup>51</sup>

## 3 Strategies for further enhancing the ionic conductivity of LAMP-based CSEs

To further improve the ionic conductivity of LAMP-based CSEs, researchers have explored multiple strategies, which can be sorted as follows.

### 3.1 Modifying LAMP fillers to optimize interfacial ion transport

The distribution of LAMP in CSEs significantly affects  $\text{Li}^+$  ion transport. Surface modification of LAMP fillers or the introduction of an interlayer can enhance the distribution of LAMP and the wettability and interactions between LAMP and the polymer matrix, reducing the interfacial resistance and facilitating ion



**Fig. 2** (a) Property comparison of solid polymer electrolytes (SPEs), inorganic solid electrolytes (ISEs), and organic–inorganic composite solid electrolytes (CSEs).<sup>5</sup> Copyright 2024, MDPI. (b) Mechanism of ion transport in PEO.<sup>56</sup> Copyright 2015, The Royal Society of Chemistry. (c) Mechanism of ion transport in PEO and inorganic fillers. The addition of inorganic fillers enhances the ion transport in inorganic–polymer composite (IPC) electrolytes (typically, poly(ethylene oxide) (PEO)-based IPCs).<sup>53</sup> Copyright 2021, with permission from Nature.



transport. In view of this, silane coupling agents are often employed as an effective means for the surface modification of inorganic nanoparticles. They enhance the compatibility between inorganic particles and polymer composites by bridging the organic/inorganic interface. For instance, Bharathi and co-workers have presented the LAMP surface modified with an amine-functionalized silane coupling agent (APTES) to enhance the interaction between PVDF-HFP and LAMP. The Lewis acid sites of LAMP were fully revealed by silane functionalization, while the antioxidant adsorption capacity of LAMP was further enhanced through electrostatic interactions with the  $-\text{NH}_3^+$  groups of APTES. A maximum ionic conductivity of  $3.01 \text{ mS cm}^{-1}$  was achieved in a PVDF-HFP/LiClO<sub>4</sub> matrix incorporating 5 wt% Si@LAMP.<sup>59</sup> Also, Wen *et al.* employed an ultrathin bifunctional coating of triaminopropyl triethoxysilane with a bifunctional structure introduced on LAMP particles, effectively bridging LAMP fillers with a PVDF-HFP/PEO polymer matrix. This approach prevented LAMP agglomeration, improved interfacial compatibility, and promoted Li<sup>+</sup> enrichment and fast transport<sup>58</sup> (Fig. 3a). In addition to the commonly used silane coupling agents mentioned above, other inorganic salt compounds have also been used to modify with the LAMP. Rong *et al.* reported LAMP particles modified with sodium itaconate (SI) to form core-shell-structured LAMP@SI, and then composited with PEO to achieve a flexible PEO-LAMP@SI CSE. By means of abundant carboxylate groups in SI nanolayers, it can not only directly provide more carriers to transport Li<sup>+</sup>, but also can cut down the interaction between Li<sup>+</sup> and the ether oxygen functional group of PEO. Also, the composite electrolytes display outstanding chemical compatibility with the Li metal anode nano-layer resulting from reduced surface energy.<sup>60</sup>

In addition to the LAMP surface modified with inorganic substances as above, some organic substances can also be used for modification. Liang *et al.* introduced a melamine

(MA) interlayer at the LAGP (a NASICON-type material like LAMP)/PEO interface. MA with a six-membered heterocyclic ring as an aromatic organic compound possesses three polar amino groups, which could serve as a transition layer to strengthen ceramic-polymer adhesion and further improve the interfacial Li<sup>+</sup> transport and mechanical properties of the composite electrolyte.<sup>61</sup> Similarly, polydopamine coated LAMP nanoparticles have been reported by He and his partners. By introducing dopamine with a good adhesion on the LAMP solid surface, it could reduce the surface energy and improve the doping proportion of LAMP in the PEO to achieve composite solid electrolytes.<sup>62</sup> This research indicates that there are three primary conduction pathways for lithium ions in this electrolyte: through the polymer chains, through the interface between the polymer and the inorganic ion conductor, and through the continuous inorganic ion conductor that forms a network/channel.

### 3.2 Incorporating ionic liquids or organic solvents as plasticizers to improve Li<sup>+</sup> migration

The addition of low-molecular-weight plasticizers or ionic liquids into the polymer matrix can reduce the glass transition temperature ( $T_g$ ) and enhance the chain segment flexibility, thereby accelerating Li<sup>+</sup> migration. For example, Zhang *et al.* used the ionic liquid 1-butyl-1-methylpyrrolidinium bis(trifluoromethylsulfonyl)imide (BMP-TFSI) into a PEO/LAMP composite electrolyte, which not only reduced the interfacial resistance between the polymer and LAMP, but also improved the ionic conductivity and lithium metal interfacial stability because it can prevent the adverse reaction between Ti<sup>4+</sup> in LAMP and Li metal.<sup>57</sup> Ma *et al.* developed a composite electrolyte consisting of LAMP particles, PEO-LiTFSI and 1-butyl-1-methylpiperidinium bis(trifluoromethylsulfonyl)imide (PP<sub>14</sub>TFSI) ionic liquid through a solvent-free procedure. Adding a small amount of ionic liquid could obviously



**Fig. 3** (a) Schematic diagram for the interaction between LAMP and APTES, and the Li<sup>+</sup> transfer pathways in SLPH. This dual functionality enables polysiloxane-modified fillers to prevent aggregation in CSEs and make close contact between the fillers and the polymer matrix.<sup>60</sup> Copyright 2025, Wiley. (b) The schematic of the PPLL and PPLLf electrolytes from configuration diagram of solid polymer electrolytes and corresponding electrochemical characteristics in lithium metal batteries and the interactions at molecular scale for PPLL and PPLLf electrolytes.<sup>66</sup> Copyright 2025, Elsevier.



enhance the interfacial contact and improve the room temperature performance. The assembled cells with this composite electrolyte revealed an improved rate and cycling performance.<sup>63</sup> Besides, ionic liquids and inorganic silane coupling agents are also used simultaneously. Wu *et al.* studied PEO-based solid-state polymer electrolytes containing a silane coupling agent and an ionic liquid grafted on the surface of LATP particles (LATP@SCA-0.25IL) by chemical grafting and ion exchange strategies. Benefiting from the synergistic effect between the protective modification layer and the coating, the interaction between PEO segments and Li<sup>+</sup> was effectively reduced, the compatibility between LATP and Li metal was enhanced, the anode performance was improved, and the dispersion of LATP in the PEO matrix was optimized, thereby accelerating Li<sup>+</sup> transfer kinetics. Given the unique modified layer, the optimized LATP particles show good stability towards Li metal and increased Li<sup>+</sup> migration, which can lead to high reversibility of Li stripping–plating over 1200 h.<sup>64</sup>

Fluoroethylene carbonate (FEC) as a commonly used additive in lithium-ion batteries is also frequently introduced into composite electrolytes to enhance ion transport. Li *et al.* incorporated FEC as an additive in a PEO/LATP system, significantly enhancing the room-temperature ionic conductivity. They proposed that FEC-derived species formed during processing contributed to improved ion transport.<sup>65</sup> Also, Zhou *et al.* discussed the addition of the fluorinated co-solvent FEC into a PEO matrix during electrolyte preparation to provide a significant effect on the free Li<sup>+</sup> transportation for ionic conduction. They used FEC as a co-solvent to improve the dispersion of the inorganic filler LATP and reduce the crystallinity of the PEO chain. In addition, FEC can weaken the binding of PEO and Li<sup>+</sup>, promote the dissociation of LiTFSI, and release more mobile Li<sup>+</sup>. Meanwhile, the addition of FEC can inhibit the growth of lithium dendrites by forming a solid electrolyte interface phase rich in LiF, demonstrating good electrochemical performance in Li||Li batteries and stable cycling performance for full cells<sup>66</sup> (Fig. 3b). Lately, Tang *et al.* employed FEC and 1,3-propane sultone (1,3-PS) as an additive to construct a PVDF-LATP composite electrolyte, which showed excellent electrochemical performance and safety with pouch cells.<sup>67</sup> Similarly, FEC and vinyl carbonate (VC) are used together to prepare a PVDF-HPF-LATP composite electrolyte, showing the cell with good interfacial compatibility and lasting inhibition of lithium dendrites. Hu *et al.* reported the *in situ* polymerization of a self-assembled nanofiber/polymer/LATP composite quasi-solid electrolyte (SL-CQSE) within a porous, flexible, and self-supporting skeleton (SSK) composed of 2-(3-(6-methyl-4-oxo-1,4-dihydropyrimidin-2-yl)ureido)ethyl methacrylate (UPyMA) self-assembled nanofibers (SAF), poly(vinylidene fluoride-co-hexafluoropropylene) (PVDF-HFP), and LATP. The precursor solution containing vinyl carbonate (VC), fluoroethylene carbonate (FEC), and lithium bis(trifluoromethanesulfonyl)imide (LiTFSI) was subjected to *in situ* polymerization. Competitive anion anchoring/hydrogen bonding and a multi-scale coupling effect among the components were found to be responsible for the SL-CQSE's non-

flammability and excellent room-temperature ionic conductivity (1.03 mS cm<sup>-1</sup>).<sup>68</sup>

### 3.3 *In situ* polymerization to facilitate fast ion transport

The *in situ* polymerization process, where liquid monomers are mixed with inorganic fillers and subsequently polymerized, can enable uniform filler dispersion and the formation of a solid electrolyte layer with close electrode contact. For example, Yi and coworkers have reported a composite electrolyte with PVDF-HFP, the poly(poly(ethylene glycol) methyl ether methacrylate-co-(lithium 2-acrylamido-2-methylpropanesulfonic acid)) (P(PEGMEMA-co-AMPSLi)) matrix, an inorganic LATP filler, and an *in situ* polymerized 1,3-dioxolane (DOL) artificial interlayer. The filler LATP and the P(PEGMEMA-AMPSLi) polymeric segments together build the fast organic–inorganic Li<sup>+</sup> ionic conducting channels. Additionally, the *in situ* formed PDOL artificial interlayer could effectively enhance the electrochemical stability of lithium metal.<sup>69</sup> In the same way, a porous PVDF-HFP membrane accommodating well-dispersed inorganic LATP particles was produced by Liu and coworkers. Subsequently, adopting *in situ* polymerized 1,3-dioxolane (PDOL) further avoids LATP from reacting with Li metal and provides a superior interfacial performance. More LATP particles can be dispersed within the PVDF-HFP porous framework *via* immersion–precipitation. Following adsorption, the subsequent *in situ* polymerization process conducted within the three-dimensional porous composite skeleton endows the solid-state battery with superior interfacial properties. The *in situ* generated PDOL layer effectively shields the reactive LATP from lithium metal. The CPE displays a high ionic conductivity of  $1.57 \times 10^{-4}$  S cm<sup>-1</sup> and oxidation stability of 5.3 V.<sup>70</sup> Recently, an *in situ* initiated poly(1,3-dioxane) (PDOL)-based gel electrolyte was developed by Yang *et al.* through infiltrating a wet-phase-induced porous polyvinylidene fluoride (PVDF) framework to stabilize the LATP/Li interface. The porous PVDF scaffold prevents direct contact between LATP and Li, effectively decoupling the rigid ceramic from the metallic anode. Internal infusion of the PDOL-based gel electrolyte enables uniform and reversible Li<sup>+</sup> deposition/stripping, thereby suppressing interfacial side reactions induced by lithium dendrite penetration. Furthermore, the ring-opening polymerization initiator Zn(OTf)<sub>2</sub> contributes to the formation of a Li–Zn alloy layer on the lithium anode, which enhances interfacial ion transport and promotes homogeneous Li<sup>+</sup> transport.<sup>71</sup>

Cao *et al.* investigated the *in situ* polymerization of 1,3-dioxolane on an LATP-coated separator, forming a dual-electrolyte system where PDOL and LATP synergistically enhanced the ionic conductivity and interfacial stability. These *in situ* approaches help mitigate issues such as filler agglomeration and poor interfacial contact encountered in conventional methods.<sup>72</sup> Reinoso *et al.* reported an alternative approach to converting the *in-situ* polymer chemical crosslinking reaction into a composite membrane electrolyte with interconnected LATP micropores by using poly(ethylene glycol) methyl methacrylate (PEG-MMA) and poly(ethylene glycol) diacrylate



(PEG-DA) as monomers and crosslinking agents through free radical initiation reactions. The test demonstrated that CSEs exhibit excellent anodic stability.<sup>73</sup> In the *in situ* polymerization of polymers, a synergistic strategy involving the introduction of ionic liquids is also employed to enhance the compatibility with LAMP and prevent adverse reactions between the lithium metal electrode and LAMP. Lin and coworkers developed a robust and elastic cross-linked PEGDA/Py<sub>13</sub>TFSI ion layer that was constructed at the interface between the electrode and the LAMP solid-state electrolyte *via* an *in situ* polymerization reaction. This approach not only significantly reduced the interfacial resistance, but also effectively suppressed adverse reactions between LAMP particles and Li metal, enabling the Li/Li symmetric cell to achieve stable cycling for over 300 hours.<sup>74</sup>

## 4 Challenges and advanced strategies for LAMP-based CSEs in solid-state batteries (SSBs)

Although LAMP-based CSEs have achieved fast development, they suffer from two critical interfacial challenges in solid-state battery applications: compatibility with lithium metal anodes and stability under high-voltage cathodes. On one hand, LAMP itself tends to undergo reduction reactions when in contact with lithium metal anodes, forming high-impedance interfacial layers that may even lead to Ti reduction and structural degradation of LAMP, significantly compromising the cycling performance and safety.<sup>75</sup> On the other hand, although LAMP intrinsically exhibits a wide electrochemical stability window (theoretically  $\sim 2.65\text{--}4.6$  V *vs.* Li/Li<sup>+</sup>),<sup>76</sup> polymer matrices (particularly PEO) limit the overall oxidative stability of CSEs. Besides, to facilitate practical applications in solid-state batteries, CSEs with both high mechanical properties and flexibility are highly desired.

### 4.1 Constructing interfacial protective layers to advance the compatibility with Li metal

The incorporation of polymer matrices can partially mitigate this issue by forming flexible interfacial layers, but it cannot completely prevent direct LAMP–lithium metal interactions.<sup>77,78</sup> To address the LAMP–lithium metal compatibility, researchers have developed various interfacial engineering strategies.

Previous studies have proposed introducing stable protective layers on LAMP surfaces or at the electrolyte–anode interface, or chemically modifying the electrode interface to prevent direct contact and suppress side reactions. These strategies aim to achieve stable operation in all-solid-state batteries.<sup>14,26</sup>

Zheng *et al.* studied the introduction of the poly(vinylene carbonate) (PVCA) and tetraethylene glycol dimethyl ether (TEGDME) protective layer into the LAMP/LiFePO<sub>4</sub> interface *via* a simple *in situ* polymerization way, and the polyvinylidene fluoride hexafluoropropylene (PVDF-HFP) and TEGDME protective layer was coated onto the LAMP surface facing the Li

anode, suppressing side reactions *via* interfacial engineering strategies.<sup>78</sup> Wen *et al.* similarly enhanced the performance of coin-type and pouch cells through interfacial modification of LAMP composite materials. The LiFePO<sub>4</sub> (LFP)||CSE||Li full cell exhibited exceptional long-term cycling stability, retaining 80% and 78% capacity after 2000 cycles at 1C and 3C rates, respectively.<sup>58</sup>

Furthermore, Liu *et al.* synthesized an organic ethylene glycol methyl ether methacrylate-*co*-acrylate acid (AAM950) polymer from LAMP and Li metal, as a protective interphase to inhibit Ti<sup>4+</sup> to Ti<sup>3+</sup> reduction and the interfacial resistance, which significantly suppresses lithium dendrite growth during charge and discharge processes.<sup>79</sup> Jin *et al.* introduced a composite polymer electrolyte at the LAMP/Li interface, which can avoid side reactions between LAMP and Li by inhibiting the formation of Li dendrites while guaranteeing high-efficiency Li ion transport (Fig. 4a).<sup>80</sup> Also, a hybrid mixed-conducting interphase (MCI) intertwined with a solid electrolyte interphase (SEI) on LAMP-PE separators was developed by Li *et al.* which can promote uniform Li deposition. This structure not only facilitates uniform lithium deposition, but also enables the Li||LFP cell to achieve stable cycling for over 200 cycles at 60 °C.<sup>81</sup> Based on this dual-protection interfacial modification strategy, the approach shows promise for universal application in high-performance, dendrite-free solid-state batteries, paving the way for future implementations.

Li *et al.* designed a 3D fiber-network-reinforced bicontinuous composite solid electrolyte with LAMP, polyacrylonitrile (PAN) and a PEO-based polymer matrix, which showed high stability and Li dendrite suppression against Li metal for all-solid-state lithium metal batteries. Meanwhile, CPEs displayed fast ionic transport due to decreasing segmental reorientations of polymers (Fig. 4c).<sup>82</sup> Choi *et al.* prepared a three-dimensional (3D) network of LAMP nanofibers to elucidate the role of the 3D LAMP network in enhancing the performance of lithium metal batteries. It was observed that the SEI structure was changed by LAMP and a LiF-enriched SEI layer was constructed.<sup>83</sup> In addition, a CSE was obtained by Ghafari and coworkers which consists of PVDF-HFP as the polymer host, tetraethylene glycol dimethyl ether (TEGDME) as the plasticizer, lithium bis(trifluoromethane)sulfonamide (LiTFSI) as the lithium salt, and LAMP as the filler. The fluorine-rich nature of the composite electrolyte facilitates the formation of a stable solid electrolyte interphase (SEI) layer on lithium-metal anodes, leading to stable cycling of Li/Li symmetric cells over 1000 h without short-circuiting.<sup>84</sup> Xue *et al.* fabricated a PEO/PVDF-HFP/5 wt% micron-sized LAMP composite electrolyte, which retained a discharge capacity of 97.9 mA h g<sup>-1</sup> (86.7% capacity retention) after 500 cycles at 0.8C in coin-cell configurations.<sup>85</sup>

In summary, significant improvements have been achieved in LAMP-based electrolytes by employing strategically engineered interfacial protective layers (*e.g.*, surface modification, compositing, additives, multilayer architectures). These approaches can effectively enhance the interfacial compatibility with electrodes/lithium metal, reduce the interfacial resis-





**Fig. 4** (a) Digital photo of pristine LAMP and CPE-coated LAMP before cycling (left two rows) and obtained from symmetric Li cells after cycling.<sup>80</sup> Copyright 2020, Elsevier. (b) Schematic diagram of the interface for mechanically assembled Si-SSLB and integrated assembled Si-SSLB.<sup>93</sup> Copyright 2025, Springer. (c) Fiber-network-reinforced composites exhibit significantly higher tensile strength, accompanied by a brilliant electrochemical stability with Li metal.<sup>82</sup> Copyright 2018, ACS. (d) Charge–discharge profile of the LFP//PIL@LAMP//Li//LFP PIL@LAMP//Li bipolar cell at 1C.<sup>89</sup> Copyright 2025, ACS. (e) Stress–strain curves for PEO-Bp and PEO-Bp-LAMP membranes.<sup>91</sup> Copyright 2019, Elsevier. (f) Nyquist plots of the composite ES-NCM||Li cell and NCM||Li cell.<sup>90</sup> Copyright 2022, Elsevier.

tance, suppress parasitic reactions, inhibit lithium dendrite growth, and improve battery safety and cycling longevity. However, these optimization strategies often require trade-offs among ionic conductivity, mechanical robustness, interfacial stability, cost, and scalability. Consequently, developing high-performance and commercially viable LAMP-based solid-state electrolytes for lithium-metal batteries remains an active research frontier, demanding further exploration of novel materials, advanced architectures, and scalable fabrication techniques.

#### 4.2 Enhancing the high-voltage stability of LAMP-based electrolytes

Synergistic polymer–filler interactions have been developed to address the high voltage of LAMP-based CSEs. Liu *et al.* proposed a straightforward strategy, which is employed to align and assemble ceramic particles. This work demonstrates that LAMP@PEGDA@PDMS self-assembles into a three-dimension-

ally interconnected network upon the application of an external AC electric field, facilitated by induced effects. Electrochemical impedance spectroscopy (EIS) confirms that the ionic conductivity of this three-dimensionally aligned network is significantly enhanced compared to its randomly oriented counterpart. It indicates that LAMP@PEGDA@PDMS is assembled into a three-dimensional connection.<sup>86</sup> Yu *et al.* set out a PEO–SN–LiTFSI dual-polymer layer with a reduction-resistant feature to ensure a stable interface at the Li anode side. At the same time, an oxidation resistant PAN–LAMP–LiTFSI polymer–ceramic composite facing the cathode enables the operation of high-capacity and high-voltage cathodes. These results indicate that the CSEs possess high ionic conductivity at room temperature and a broad electrochemical stability window of 0–5 V.<sup>87</sup> Recently, Chen *et al.* proposed a thin and flexible hybrid electrolyte comprising LAMP and poly(vinylidene fluoride-trifluorethylene) (PVDF-TrFE) incorporated with a highly concentrated ionic liquid electrolyte (ILE) to



achieve an enhanced high voltage stability through LATP filler-assisted lithium salt dissociation.<sup>88</sup> Choi *et al.* synthesized a polymer ionic liquid (PIL) with high ionic conductivity through an anion exchange reaction and employed it as a coating layer on LATP. Surprisingly, the stacked bipolar cell demonstrated notable voltage performance with an operational voltage reaching approximately 6.7 V (Fig. 4d).<sup>89</sup> The aforementioned results demonstrate that the optimized LATP-based CSE exhibits a wide electrochemical stability window and excellent compatibility/interface stability with medium-voltage cathodes (*e.g.*, LFP).

In contrast, direct applications of LATP-based CSEs in high-voltage  $\text{LiNi}_x\text{Co}_y\text{Mn}_{(1-x-y)}\text{O}_2$  (NCM) cathode systems remain relatively scarce. Liang *et al.* developed a MA-modified PEO-MA@LAGP CSE and assembled Li/PEO-MA@LAGP/NCM523 cells, achieving a fivefold enhancement in cycle life compared to the PEO-LAGP-based counterparts.<sup>61</sup> Tang *et al.* constructed an NCM622||LE-LATP membrane-LE||Si/C coin cell using an LATP composite membrane, reporting an initial discharge capacity of  $\sim 163 \text{ mA h g}^{-1}$  (0.5C, 25 °C) with 87% capacity retention after 100 cycles. Notably, a 5 Ah NCM622||LE-LATP membrane-LE||Si/C pouch cell retained >90% capacity over 400 cycles (1C, 25 °C).<sup>67</sup> Cao *et al.* applied an LATP-coated separator to NCM811||Li cells, achieving 82.1% capacity retention after 500 cycles (1C, 25 °C), underscoring the potential of LATP-based systems for high-voltage applications.<sup>72</sup> Similarly, Jin's team designed an ES-NCM||LATP-PVDF||Li cell, which delivered a high areal capacity of  $1.19 \text{ mA h cm}^{-2}$  under an ultrahigh ES-NCM loading ( $9.28 \text{ mg cm}^{-2}$ ), further validating the feasibility of composite electrolytes paired with high-loading cathodes for high-energy-density solid-state lithium batteries (SSLBs) (Fig. 4f).<sup>90</sup>

By leveraging composite additives and chemical modifications, the synergistic interplay between organic polymers and inorganic LATP materials was precisely engineered. This strategy not only broadened the electrolyte's voltage window to meet the stringent demands of high-voltage systems, but also addressed critical challenges in developing LATP-based composite electrolytes for next-generation SSLBs.

### 4.3 Synergistic optimization of mechanical properties and flexibility of LATP-based CSEs

The LATP composite electrolyte synergistically optimizes mechanical strength and flexibility by dispersing high-modulus LATP fillers within a compliant polymer matrix. For instance, Zhu *et al.* developed a polymer-in-ceramic composite electrolyte that combines exceptional flexibility ( $\sim 300\%$  elongation) with robust mechanical integrity.<sup>51</sup> Equally, Li *et al.* demonstrated that fiber-network-reinforced composites exhibit significantly higher tensile strength than pure PEO electrolytes, accompanied by a brilliant electrochemical stability towards Li metal lasting for 15 days and an enlarged tensile strength even reaching 10.72 MPa.<sup>82</sup> Also, a new composite gel polymer electrolyte (PEO-Bp-LATP) including polyethylene oxide (PEO), benzophenone (Bp) and LATP was pre-

pared using significant ultraviolet (UV) technology by Syal and their workers. The PEO-Bp-LATP composite electrolyte not only show a wider electrochemical stability window >5 V, but also has a good mechanical strength of 9.3 MPa (Fig. 4e).<sup>91</sup> Dong *et al.* reported a polymer electrolyte matrix with LATP and glass fiber (GF) as reinforcement fillers; the LATP-GF-PEO composite electrolyte developed offers a high tensile strength of 33.1 MPa, along with a large  $\text{Li}^+$  transfer number of 0.37.<sup>92</sup> Liu *et al.* prepared the PVDF-HFP/LATP composite electrolyte, combined with the Si anode loaded with LATP, which showed a tensile strength of 2.0 MPa and the tensile strain at break of 22.8%.<sup>93</sup> These results suggest that the composite electrolyte possesses excellent mechanical strength and can mitigate the volume expansion of the anode.

In addition to lithium metal, silicon anodes have attracted significant attention due to their ultrahigh theoretical capacity but they suffer from severe volume expansion. Han *et al.* designed highly dense Ag nanoparticles decorated with porous micronized Si and coated with thin-layer carbon (PS-Ag-C) to decrease the large volume change of Si. Besides, they were coupled with PVDF-HFP/ $\text{Li}_{1.3}\text{Al}_{0.3}\text{Ti}_{1.7}(\text{PO}_4)_3$  (LATP) to form a LiF-rich SEI, which can ensure desirable interfacial and mechanical stability. The full cell assembled by pairing the PS-Ag-C anode with the NCM811 cathode displayed a high initial reversible capacity of  $213.6 \text{ mA h g}^{-1}$  and when cycled at a high density current ( $1 \text{ A g}^{-1}$ ), it still maintained  $130.2 \text{ mA h g}^{-1}$  over 200 cycles.<sup>94</sup> Liu and some researchers recently proposed the PEO/PVDF-HFP/LATP composite electrolyte, possessing the good flexibility of the composite, which tends to adaptively change its structure with the expansion/contraction of silicon, ensuring the rapid transfer of interface ions. Their Si||LFP full cell retained 81% of its capacity after 100 cycles, highlighting the effectiveness of the LATP composite in mitigating silicon anode degradation.<sup>73</sup> Specifically, Liu and colleagues reported that this battery, integrating a silicon anode, PVHS-LCSE, and a LFP cathode, delivered a discharge specific capacity of  $122.6 \text{ mA h g}^{-1}$  after 100 cycles, with a capacity retention rate of 81.5% (Fig. 4b).<sup>93</sup> This balanced integration of flexibility and mechanical strength guarantees that LATP composite electrolytes not only enhance the battery performance, but also maintain stable interfacial contact during electrode volume fluctuations, while remaining compatible with scalable production methods. Such properties make them promising candidates for practical solid-state battery applications.

In summary, LATP composite electrolytes have demonstrated promising performance across diverse solid-state battery configurations, achieving remarkable cycling stability and rate capability through optimized composition, microstructure, and interfacial design. However, further advancements are needed to match or surpass the energy density and cycle life of conventional liquid lithium-ion batteries, particularly under room-temperature operation and in high-voltage/high-loading systems, which would require subsequent research into material engineering and interface optimization (Table 1).





**Table 1** Summary of recent developments in LATP-based composite electrolytes

| Electrolyte composition                     | Ionic conductivity ( $\text{mS cm}^{-1}$ ) | Battery type   | Mass loading ( $\text{mg cm}^{-2}$ ) | Cycling stability (voltage, CR, cycles, rate/density, CE)                          | Ref. |
|---|--|----------------|--------------------------------------|--|------|
| LATP-PEO                                    | 0.173, 25 °C                               | Li/LFP         | 1.3                                  | 2.8 V-4.0 V, 97.3%, 100 cycles, 0.3C, 99.9%, RT                                    | 18   |
| PVDF-LATP                                   | 0.626, 30 °C                               | Li/LMO         | —                                    | 3 V-4.3 V, 91.4%, 200 cycles, 0.2C, nearly 100%, RT                                | 21   |
| LATP/PVDF (2:1)                             | 0.967, 25 °C                               | Li/LFP         | —                                    | 2.5 V-4.2 V, 90.1%, 200 cycles, 0.1C, nearly 100%, RT                              | 32   |
| PAN/30 wt%LATP                              | 1.7, RT                                    | Li/LFP         | 5                                    | 2.5 V-4.2 V, 87%, 200 cycles, 0.5C, 96.5%, RT                                      | 33   |
| 700-PAN/O-LATP                              | 0.755, 20 °C                               | Li/LFP         | 1                                    | 2.0 V-4.5 V, 95.6%, 100 cycles, 0.1C, nearly 100%, 25 °C                           | 34   |
| AHPAA-PEO-LITFSI                            | 0.179, 30 °C                               | Li/LFP         | —                                    | 2.8 V-3.85 V, 91%, 2023 cycles, 1C, nearly 100%, 50 °C                             | 35   |
| PEO@BPIL-3-SPE                              | 0.22, 60 °C                                | Li/LFP         | 1.8-3                                | 2.8 V-4.2 V, 81%, 50 cycles, 0.2C, 98%, 60 °C                                      | 38   |
| 15%LATP/PAN EC/EMC                          | 0.131, RT                                  | Li/NMC811      | —                                    | 2.5 V-4.2 V, 91%, 50 cycles, 0.2C, RT  | 39   |
| PEO-SN-PAN/LATP                             | 0.124, 30 °C                               | Li/NMC811      | 3.0-4.0                              | 2.5 V-4.5 V, 91%, 300 cycles, 0.2C, 98.8-100%, RT                                  | 40   |
| PI/PEO/LATP                                 | 0.187, 60 °C                               | Li/NMC811      | —                                    | 95%, 100 cycles, 0.2C, nearly 100%, 30 °C  | 41   |
| PMMA/PEO/PVDF-HFP                           | 0.187, 60 °C                               | Li/LFP         | 2-3                                  | 3.0 V-4.0 V, 95.7%, 200 cycles, 0.5C, 60 °C  | 43   |
| LATP/PAN/PEO                                | 0.626, 60 °C                               | Li/NCM811      | 2-3                                  | 3.0 V-4.3 V, 90%, 100 cycles, 0.5C, 60 °C  | 44   |
| PAN/MOFs/ILs-PEO                            | 0.437, RT                                  | Li/NCM622      | 3                                    | 2.8 V-4.3 V, 89%, 120 cycles, 0.5C, 99.5%, 60 °C                                   | 45   |
| PEO-LATP@SI-6                               | 0.115, 30 °C                               | Li/LFP         | 1.5-4                                | 2.5 V-4.0 V, 90.1%, 2100 cycles, 1C, nearly 100%, 60 °C                            | 45   |
|   | 1.2, 60 °C                                 | Li/LFP         | ~2.0                                 | 2.9 V-3.8 V, 88.5%, 100 cycles, 0.2C, 98.7%, 60 °C                                 | 60   |
|   | 120 $\mu\text{m}$                          | Li/NCM523      | —                                    | 3.0 V-4.3 V, 90.9%, 35 cycles, 0.2C, 98%, 60 °C                                    | 60   |
| PEO <sub>0.2</sub> -PAD@LATP <sub>0.8</sub> | 0.207, 30 °C                               | Li/NCM811      | 9.1                                  | 3.0 V-4.2 V, 96.7%, 200 cycles, 0.2C, 30 °C  | 62   |
|   | 2.05, 80 °C                                |                | —                                    |  |      |
| PEO-LATP-3 wt%IL                            | 0.01, 25 °C                                | Li/LFP         | —                                    | 2.8 V-4.0 V, 97.8%, 150 cycles, 1C, 60 °C  | 63   |
| LATP@SCA-0.25IL                             | 1.455, 60 °C                               | Li/LFP         | ~1.9                                 | 2.9 V-3.8 V, 83.9%, 120 cycles, 0.2C, 60 °C  | 64   |
| PEO-LATP                                    | 0.199, 30 °C with FEC                      | Li/NCM811      | 2.0                                  | 3.0 V-3.8 V, 89.7%, 300 cycles, 0.2C, 25 °C  | 65   |
| PEO-PAN-LiTFSI-LATP                         | 0.1, RT with 5 wt% FEC                     | Li/LFP         | 1.5-2.0                              | 2.8 V-3.9 V, 85.3%, 500 cycles, 0.5C, 50 °C  | 66   |
| SAF-PVDF-HFP-LATP                           | 1.03, RT with FEC, VC                      | Li/LFP         | 1.6                                  | 2.5 V-4.2 V, 90.4%, >1000 cycles, 1C, RT   | 67   |
| (P(PEGMEMA-co-AMPSLi))-LATP-PDOL            | 0.347, RT (PPAL5-D)                        | Li/LFP         | 2.6 ± 0.2                            | 2.5 V-4.2 V, 78.3%, 400 cycles, 1C, 99.5%, 25 °C                                   | 69   |
|   |  | Li/NCM811      | 2.8 ± 0.2                            | 2.7 V-4.3 V, 86.7%, 100 cycles, 0.5C, 25 °C  |      |
| PVDF-HFP-LATP-PDOL                          | 0.157, RT 60 $\mu\text{m}$                 | Li/LFP         | ~1.5                                 | 2.5 V-4.3 V, 97.72%, 300 cycles, 1.0C, 99.9%, 25 °C                                | 70   |
| PVCA-LATP-PVDF-HFP                          | >0.1, 25 °C                                | Li/LFP         | ~1.6-1.8                             | 2.8 V-4.0 V, 89.9%, 300 cycles, 0.5C, 60 °C  | 78   |
| LATP/AAM950                                 | 0.93, RT                                   | Li/NCM622      | —                                    | 2.0 V-4.2 V, 80.4%, 100 cycles, 0.1C, RT   | 79   |
| PEO-LiTFSI-LATP-PE                          | 0.14, 60 °C                                | Li/LFP         | ~1.5                                 | 3.0 V-3.8 V, 103.5%, 200 cycles, 0.2C, 60 °C                                       | 81   |
| LATP-PAN                                    | 0.749, RT                                  | Li/NCM811      | 5                                    | 3.0 V-4.2 V, 88%, 200 cycles, 0.2C, RT   | 83   |
| PVDF-HFP-TEGDEM-LITFSI-LATP                 | 0.317, RT 100 $\mu\text{m}$                | Li/LFP         | 5                                    | 2.6 V-4.3 V, 80%, 648 cycles, 0.5C, RT   | 84   |
| PEO-SN-LITFSI/PAN-LATP-LITFSI               | 0.131, RT 200 $\mu\text{m}$                | Li/NCM811      | 3.0-4.0,                             | 2.6 V-4.4 V, 91%, 300 cycles, 0.2C, 98.8-100%                                      | 87   |
| LATP/PVD-TrFE/ILE                           | 0.31, 20 °C                                | Li/NCM811      | 2.5 ± 0.1,                           | 3.0 V-4.3 V, 83.5%, 150 cycles, 0.5C, 20 °C  | 88   |
| PEO-Bp-15 wt% LATP                          | 3.3, RT                                    | Li/LFP         | —                                    | 2.7 V-4.2 V, 84%, 200 cycles, 0.1C, RT   | 91   |
| PIL@LATP                                    | 0.11, 30 °C                                | Li/LFP         | 2.4                                  | 2.7 V-4.0 V, 87.3%, 200 cycles, 1C   | 89   |
| PVDF-HFP/SN/LATP                            | 0.12, 60 °C                                | Li/Si-LA       | —                                    | 0 V-2.0 V, 40.3%, 200 cycles, 1C   | 93   |
| PVDF-HFP-LATP                               | —  | Li/Si-Ag-C     | 2.3                                  | 0.005 V-1.5 V, 4.0 mA h $\text{cm}^{-2}$ after 100 cycles at 0.5 A $\text{g}^{-1}$ | 93   |
|   |  | Si-Ag-C/NCM811 | N/P = 1.1/1                          | 2.5 V-4.4 V, 60.96%, 200 cycles, 0.5 A $\text{g}^{-1}$                             | 94   |

## 5 Summary and future perspectives

Compared to traditional lithium-ion batteries, all-solid-state lithium metal batteries exhibit higher theoretical energy density, enhanced safety, and superior cycling stability, making them worth extensive research in both academia and industry.<sup>95,96</sup> Although LATP-based CSEs present a promising solution for developing high-performance all-solid-state lithium batteries, the development and large-scale application of high-performance all-solid-state metal batteries still face numerous challenges, including incompact/unstable electrolyte–electrode interfaces, sluggish Li<sup>+</sup> transport kinetics, and persistent lithium dendrite growth.<sup>97,98</sup> Future research should prioritize the use of advanced characterization techniques to elucidate the intricate chemo–electrochemical–mechanical interactions in composite solid-state electrolytes and uncover interfacial reactions and failure mechanisms to provide theoretical guidance for the design and innovation of high-performance electrolyte materials, thereby accelerating the iterative development of all-solid-state battery technologies (Fig. 5).

### 5.1 Interfacial challenges remain a critical bottleneck

Polymer-based electrolytes, as one of the core components of all-solid-state batteries, have attracted widespread attention due to their excellent compatibility with lithium metal anodes.<sup>99,100</sup> However, composite electrolyte systems based on LATP ceramics and polymer matrices still face two critical challenges in practical applications: poor interfacial contact and electrochemical instability between the electrolyte and lithium metal, which severely limit the overall ionic conductivity of composite electrolytes and the cycling stability of all-solid-state batteries.<sup>60,101,102</sup> Although interfacial engineering strategies (e.g., surface modification, interlayer construction, or additive incorporation) can partially mitigate these interfacial issues, constructing an ideal solid–solid interface with low interfacial impedance, high interfacial stability, and good volume adaptability remains a significant challenge.<sup>103–105</sup> Future research should focus on employing advanced characterization techniques to fundamentally elucidate the correlation between interfacial structure evolution and electrochemical behavior in composite electrolytes. For instance, emerging confocal Raman imaging and *in situ* Raman techniques enable the visualization of three-dimensional stress distribution, thereby

revealing the relationship between stress evolution and material crack propagation.<sup>106–108</sup> Also, *in situ* X-ray micro-computed tomography (X-ray micro CT) has been widely used to study how the continuous growth of interfacial phases at the lithium cathode–solid electrolyte interface promotes the initiation and propagation of cracks in solid electrolytes.<sup>109,110</sup> Furthermore, integrating multimodal characterization methods not only allows for synchronous acquisition of chemical composition information within batteries, but also systematically uncovers the mechanisms of ion transport and the nature of interfacial side reactions. Sun and co-workers adopted electrochemical impedance spectroscopy (EIS) along with *in situ* XCTM to analyze electrochemical–mechanical coupling. Meanwhile, time-of-flight secondary-ion mass spectrometry (TOF-SIMS) and finite element analysis (FEA) modeling are jointly used to decouple the electro–chemo–mechanical coupling.<sup>111</sup> By the way, to investigate the changes in the electrode–electrolyte interface at a finer scale, transmission electron microscopy (TEM), a widely utilized imaging technique, has been employed by researchers. Li and coworkers have studied the interface reactions and structural changes of electrolytes/lithium in solid-state lithium-metal batteries (SSLMBs) at the nanoscale are visualized by *in situ* transmission electron microscopy (TEM), revealing minimal morphological alterations of LAGP@P-DOL particles during charge and discharge processes. Cryo-TEM and TOF-SIMS combinedly confirm the formation of a LiF-rich interfacial layer at the LAGP@P-DOL/Li interface, which promotes uniform Li ion distribution and facilitates dense, homogeneous lithium deposition.<sup>112</sup> Lately, Gao *et al.* proposed such an attempt by observing the exfoliation and plating interfaces of micron-sized SSLMBS cycling in constant current mode under a transmission electron microscope. The various voltage responses in the charge–discharge curve are closely related to the nucleation, growth and reflation of individual voids.<sup>113</sup> These insights will provide theoretical support for the interfacial optimization and material design of all-solid-state batteries, accelerating their practical application in high-energy-density battery systems.

### 5.2 Room-temperature ionic conductivity needs further improvement

The composite electrolyte strategy, which combines inorganic conductive materials with a polymer matrix, effectively over-

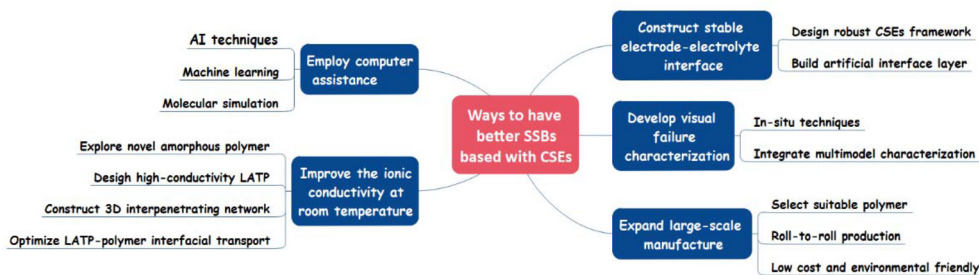


Fig. 5 Strategies for mass-producible solid-state batteries based on CSEs.



comes the limitations of single-component electrolytes, thereby meeting the multifaceted physicochemical requirements for high-performance all-solid-state batteries.<sup>114,115</sup> However, current LTP-based composite solid electrolytes still exhibit significantly lower ionic conductivity than liquid electrolytes at room temperature, particularly under high-rate charge/discharge conditions, where ion transport limitations become more pronounced.<sup>116–118</sup> To address these challenges, future research should prioritize the following directions: (1) exploring novel amorphous polymer-based electrolytes; enhancing the intrinsic conductivity and stability of polymer matrices through molecular design and structural optimization; (2) optimizing polymer–LTP interfacial interactions; suppressing interfacial side reactions and improving the interfacial ion transport efficiency; (3) designing high-conductivity doped LTP fillers; boosting the ionic conductivity and interfacial compatibility of inorganic fillers *via* elemental doping or structural modification; (4) constructing three-dimensional (3D) interpenetrating network-structured composite electrolytes; diversifying and stabilizing ion transport pathways to enhance the rate capability and cycling longevity. Advancing these research directions will provide critical support for improving the ionic conductivity of solid electrolytes and the rate performance of all-solid-state batteries, accelerating their practical application in high-energy-density scenarios.

### 5.3 Dendrite suppression requires enhanced mechanical and interfacial design

Although composite solid-state electrolytes enhance mechanical strength by incorporating inorganic fillers (*e.g.*, LTP) and suppress lithium dendrite growth through physical barrier layers or chemically compatible interfacial components, completely preventing dendrite penetration under high current densities and long-term cycling remains a critical challenge.<sup>80,119,120</sup> Therefore, future research should focus on synergistic strategies that combine bulk mechanical reinforcement with interfacial engineering to improve the electrolyte/lithium metal compatibility and reduce the interfacial impedance. Specifically, these efforts include: (1) constructing mechanically robust composite frameworks: designing rigid or flexible 3D network skeletons can enhance the structural stability of electrolytes, effectively buffering volume changes and inhibiting dendrite propagation. (2) Precise interfacial modification: artificially engineered interlayers with ion/electron-conducting properties (*e.g.*, tailored SEI layers) can form stable buffer structures between the electrolyte and lithium metal, guiding uniform Li deposition and facilitating the formation of dense, stable solid electrolyte interphases (SEIs).<sup>58,121,122</sup> Through such synergistic approaches, superior interfacial compatibility between electrolytes and anodes can be achieved, promoting homogeneous lithium deposition/stripping and ultimately improving battery safety and cycling stability. This paves the way for advancing high-safety all-solid-state lithium metal batteries.

### 5.4 Scalable manufacturing is key to commercialization

Currently, most high-performance LTP-based composite electrolytes are prepared *via* lab-scale methods, yet they often suffer from limitations such as insufficient ionic conductivity and inadequate high-voltage stability.<sup>123</sup> Although externally applied pressure can improve interfacial contact and enhance the performance, this approach largely hinders the large-scale, cost-effective industrialization of all-solid-state batteries and remains incompatible with mass-production processes. Thus, achieving reliable and scalable manufacturing of solid-state electrolytes is a critical challenge to address. Future efforts should prioritize the development of economically viable, environmentally friendly, and scalable advanced production technologies. Recently, Yi and coworkers developed a multifunctional polyethylene separator (S7540) achieving a perfect balance between ultra-high porosity (75%) and wide pore size distribution. When combining with PEO–LTP as a composite electrolyte, this CSE demonstrates brilliant mechanical integrity, enhancing the mechanical properties of the PEO composite solid electrolyte by nearly 50 times (with a tensile strength of 42.11 MPa). The Li/LiCoO<sub>2</sub> system equipped with this CSE shows ultra-high cycling stability at a 10C (6.2 mA h cm<sup>-2</sup>), significantly surpassing traditional commercial separators. What's more, it is particularly important that the CSE is seamlessly compatible with existing liquid/solid battery production lines, with powerful potential for large-scale production.<sup>124</sup> Key directions include: (1) selecting suitable polymer electrolyte components, prioritizing polymer matrices with excellent scalability (*e.g.*, solution processability), strong interfacial compatibility with electrode materials, and sustainable, cost-controllable raw material sources. (2) Developing mature industrial-scale fabrication processes, exploring and optimizing low-cost, high-throughput methods for mass production, such as roll-to-roll continuous manufacturing or *in situ* polymerization techniques. These approaches enable synchronous construction of electrolytes and electrodes, significantly reducing production costs while maintaining superior electrochemical performance.<sup>125,126</sup>

### 5.5 Computational guidance can accelerate development

Preliminary theoretical models have been established to describe the ionic transport properties of solid-state electrolytes, dendrite growth dynamics, and battery failure mechanisms.<sup>127–129</sup> However, the multiscale microstructure of composite materials and the complexity of multiphase interfaces make it challenging for existing theories to fully elucidate the underlying mechanisms. To address these challenges, first-principles calculations and density functional theory (DFT) can be employed to probe the electronic structure, lattice dynamics, and interfacial properties at the atomic scale, providing insights into ion transport pathways, energy barriers, and the impact of defect engineering on performance. Meanwhile, molecular dynamics simulations, combined with force fields or quantum mechanical methods, can dynamically depict lithium-ion migration, solvation structure evolution,



and dendrite growth processes, offering mechanistic guidance for dendrite suppression.<sup>130–132</sup>

Additionally, machine learning (ML) and artificial intelligence (AI) techniques, particularly high-throughput computing and machine learning potentials, enable rapid screening of candidate materials with superior ionic conductivity, wide electrochemical stability windows, and excellent mechanical and chemical compatibilities.<sup>133,134</sup> By establishing mapping relationships between input parameters (*e.g.*, composition, structure, temperature) and output performance, AI can guide experimental design, significantly reducing costs and accelerating material discovery.

All-solid-state batteries are regarded as a pivotal direction for next-generation battery technologies due to their advantages in high energy density and enhanced safety. However, transitioning from laboratory research to industrial-scale applications remains a formidable challenge. To accelerate this transition, deep collaboration between fundamental research and industry is imperative, spanning theoretical advancements, material innovation, and process optimization. Such synergistic efforts hold promise for overcoming critical barriers in the rapid development of all-solid-state batteries, ultimately enabling high-performance composite solid electrolytes to bridge the gap between laboratory breakthroughs and large-scale industrialization.

In summary, future research should prioritize precise control of composite composition and microstructure, in-depth understanding and optimization of multiphase interfacial characteristics, development of efficient and scalable manufacturing techniques, and enhanced integration of computational modeling with experimental studies. By addressing these critical aspects, we can overcome existing challenges and accelerate the commercialization of LATP composite electrolytes and all-solid-state battery technologies, ultimately delivering safer and higher-energy-density power sources for electric vehicles and large-scale energy storage applications.

## Author contributions

This manuscript was completed by all the authors together. All the authors have approved the final version of the manuscript.

## Conflicts of interest

The authors declare no competing financial interest.

## Data availability

No primary research results, software or code have been included and no new data were generated or analysed as part of this review.

## Acknowledgements

This work was supported by the Jiangsu Provincial Science and Technology Program (Major Project) [Grant No. BG 2024020], the National Key R&D Program of China (Grant No. 2022YFE0207300) and the National Natural Science Foundation of China (Grant No. 22179142). Also, we gratefully acknowledge the support of the Jiangsu Funding Program for Excellent Postdoctoral Talent (Grant No. 2025ZB399, No. 2025ZB813) for this work.

## References

- J. M. Tarascon and M. Armand, *Nature*, 2001, **414**, 359–367.
- M. Armand and J. M. Tarascon, Building better batteries, *Nature*, 2008, **451**, 652–657.
- A. Manthiram, X. W. Yu and S. F. Wang, *Nat. Rev. Mater.*, 2017, **2**, 16103.
- P. G. Bruce, S. A. Freunberger, L. J. Hardwick and J. M. Tarascon, *Nat. Mater.*, 2011, **11**, 19–29.
- S. Ai, X. Wu, J. Wang, X. Li, X. Hao and Y. Meng, *Nanomaterials*, 2024, **14**, 1773.
- X. Zhan, M. Li, X. L. Zhao, Y. N. Wang, S. Li, W. W. Wang, J. D. Lin, Z.-A. Nan, J. W. Yan, Z. F. Zhe, H. D. Liu, F. Wang, J. Y. Wan, J. J. Liu, Q. B. Zhang and L. Zhang, *Nat. Commun.*, 2024, **15**, 1056.
- C. H. Chan, H. H. Wong, S. P. Liang, M. Z. Sun, T. Wu, Q. Y. Lu, L. Lu, B. A. Chen and B. L. Huang, *Batteries Supercaps*, 2024, **7**, e202400432.
- S. Khan, I. Ullah, M. U. Rahman, H. Khan, A. B. Shah, R. H. Althomali and M. M. Rahman, *Rev. Inorg. Chem.*, 2024, **44**, 347–375.
- H. Lukas, F. William, S. Silvan, B. Debbie, W. M. Steve, W. Martin and B. Peter, *Batteries Supercaps*, 2024, **7**, e202300478.
- B. E. Francisco and C. R. Stoldt, *Chem. Mater.*, 2014, **26**, 4741–4749.
- R. DeWees and H. Wang, *ChemSusChem*, 2019, **12**, 3713–3725.
- D. Zhang, X. Xu, Y. Qin, S. Ji, Y. Huo, Z. Wang, Z. Liu, J. Shen and J. Liu, *Chem. – Eur. J.*, 2019, **26**, 1720–1736.
- R. Shah, V. Mittal and A. M. Precilla, *J.*, 2024, **7**, 204–217.
- K. Yang, L. K. Chen, J. B. Ma, Y.-B. He and F. Y. Kang, *InfoMat*, 2021, **3**, 1–23.
- A. Jonderian and E. McCalla, *Mater. Adv.*, 2021, **2**, 2846–2875.
- M. Avdeev, *Chem. Mater.*, 2021, **33**, 7620–7632.
- X. Han, Y. Gong, K. Fu, X. He, G. T. Hitz, J. Dai, A. Pearse, B. Liu, H. Wang, G. Rubloff, Y. Mo, V. Thangadurai, E. D. Wachsman and L. Hu, *Nat. Mater.*, 2017, **16**, 572–579.
- Z. Yang, H. Yuan, C. Zhou, Y. Wu, W. Tang, S. Sang and H. Liu, *Chem. Eng. J.*, 2020, **392**, 123650.



- 19 Z. X. Lin, O. W. Sheng, X. H. Cai, D. Duan, K. Yue, J. W. Nai, Y. Wang, T. F. Liu, X. Y. Tao and Y. J. Liu, *J. Energy Chem.*, 2023, **81**, 358–378.
- 20 Y. W. Chen-Yang, H. C. Chen, F. J. Lin and C. C. Chen, *Solid State Ionics*, 2002, **150**, 327–335.
- 21 X. H. Liang, D. Han, Y. T. Wang, L. X. Lan and J. Mao, *RSC Adv.*, 2018, **8**, 40498–40504.
- 22 S. H. Wang, A. L. Monaca and G. P. Demopoulos, *Energy Adv.*, 2025, **4**, 11–36.
- 23 R. Chen, Q. Li, X. Yu, L. Chen and H. Li, *Chem. Rev.*, 2020, **120**, 6820–687723.
- 24 T. F. Zhang, W. J. He, W. Zhang, T. Wang, P. Li, Z. M. Sun and X. B. Yu, *Chem. Sci.*, 2020, **11**, 8686–8707.
- 25 H. W. Zhai, P. Y. Xu, M. Q. Ning, Q. Cheng, J. Mandal and Y. Yang, *Nano Lett.*, 2017, **17**, 3182–3187.
- 26 Z. Y. Zou, Y. J. Li, Z. H. Lu, D. Wang, Y. H. Cui, B. K. Guo, Y. G. Li, X. M. Liang, J. W. Feng, H. Li, C.-W. Nan, M. Armand, L. Q. Chen, K. Xu and S. Q. Shi, *Chem. Rev.*, 2020, **120**, 4169–4221.
- 27 S. L. Liu, W. Y. Liu, D. L. Ba, Y. Z. Zhao, Y. H. Ye, Y. Y. Li and Ji. P. Liu, *Adv. Mater.*, 2023, **35**, 21103.
- 28 X. Y. Yang, J. X. Liu, N. B. Pei, Z. Q. Chen, R. Y. Li, L. J. Fu, P. Zhang and J. B. Zhao, *Nano-Micro Lett.*, 2023, **15**, 74.
- 29 P. V. Wright, *Br. Polym. J.*, 1975, **7**, 319–327.
- 30 S. Bonizzoni, C. Ferrara, V. Berbenni, U. Anselmi-Tamburini, P. Mustarelli and C. Tealdi, *Phys. Chem. Chem. Phys.*, 2019, **21**, 6142–6149.
- 31 S. S. Sekhon and H. P. Singh, *Solid State Ionics*, 2002, **152–153**, 169–174.
- 32 X. J. Shi, N. Y. Ma, Y. X. Wu, Y. H. Lu, Q. Z. Xiao, Z. H. Li and G. T. Li, *Solid State Ionics*, 2018, **325**, 112–119.
- 33 J. Mohanta, O. H. Kwon, J. H. Choi, Y.-M. Yun, J.-K. Kim and S. M. Jeong, *Nanomaterials*, 2019, **9**, 1581.
- 34 X. Gu, Q. Wu, Y. Cai, Y. Wu, Q. Jiang, Y. Li, H. Tian, X. Yao and Z. Su, *Ceram. Int.*, 2024, **50**, 10137.
- 35 W. Liu, G. Li, W. Yu, L. Gao, D. Shi, J. Ju, N. Deng and W. Kang, *Energy Storage Mater.*, 2023, **63**, 103005.
- 36 G. Zardalidis and F. Farmakis, *Adv. Energy Mater.*, 2023, **13**, 2301035.
- 37 J. Yang, C. Yi, M. Li, Z. Wu, J. Xia, Y. Li and J. Liu, *Energy Environ. Mater.*, 2025, e70090.
- 38 X. Zhu, Z. Fang, Q. Deng, Y. Zhou, X. Fu, L. Wu, W. Yan and Y. Yang, *ACS Sustainable Chem. Eng.*, 2022, **10**, 4173–4185.
- 39 Y. Z. Liang, Z. Lin, Y. P. Qiu and X. W. Zhang, *Electrochim. Acta*, 2011, **56**, 6474–6480.
- 40 X. Yu, J. Li and A. Manthiram, *ACS Mater. Lett.*, 2020, **2**, 317–324.
- 41 L. He, W. H. Liang, J. H. Cao and D. Y. Wu, *ACS Appl. Energy Mater.*, 2022, **5**, 5277.
- 42 N. J. Shah, M. Shalaby, L. He, X. Wang, D. Deslandes, B. A. Garetz and N. P. Balsara, *ACS Macro Lett.*, 2023, **12**, 874.
- 43 J. Wang, Y. Zhang, Z. Chen, S. Fan, Q. Zhang, Y. Zhang, T. Zhang, C. Zhang and Q. Chi, *Chem. Eng. J.*, 2024, **492**, 152222.
- 44 J. Y. Liang, X. X. Zeng, X. D. Zhang, T. T. Zuo, M. Yan, Y. X. Yin, J. L. Shi, X. W. Wu, Y. G. Guo and L. J. Wan, *J. Am. Chem. Soc.*, 2019, **141**, 9165.
- 45 L. Q. Liu, L. F. Zhu, Y. L. Wang, X. W. Guan, Z. F. Zhang, H. Li, F. Wang, H. Zhang, Z. Zhang, Z. Y. Yang and T. Y. Ma, *Angew. Chem., Int. Ed.*, 2025, **64**, e202420001.
- 46 E. Trevisanello, T. Ates, S. Passerini, F. H. Richter and J. Janek, *J. Electrochem. Soc.*, 2022, **169**, 110547.
- 47 C. L. Li, J. Wang, Z. W. Chang, Y. B. Yin, X. Y. Yang and X. B. Zhang, *Sci. Sin.: Chim.*, 2018, **48**, 964–971.
- 48 L. Q. Wu, Y. T. Wang, X. W. Guo, P. P. Ding, Z. Y. Lin and H. J. Yu, *SusMat*, 2022, **2**, 264–292.
- 49 S. X. Xia, X. S. Wu, Z. C. Zhang, Y. Cui and W. Liu, *Chem.*, 2019, **5**, 753–785.
- 50 H. Kim, M. R. Shaik, S. Kim, Y. M. Park, D. W. Jeon, S. B. Cho, S. Choi and W. B. Im, *Int. J. Energy Res.*, 2024, **1**, 116417.
- 51 L. Zhu, J. C. Chen, Y. W. Wang, W. L. Feng, Y. Z. Zhu, S. F. H. Lambregts, Y. M. Wu, C. Yang, E. R. H. van Eck, L. M. Peng, A. P. M. Kentgens, W. P. Tang and Y. Y. Xia, *J. Am. Chem. Soc.*, 2024, **146**, 6591–6603.
- 52 W. Yu, N. P. Deng, D. J. Shi, L. Gao, B. W. Cheng, G. Li and W. M. Kang, *ACS Nano*, 2023, **17**, 22872–22884.
- 53 L.-Z. Fan, H. C. He and C.-W. Nan, *Nat. Rev. Mater.*, 2021, **6**, 1003–1019.
- 54 M. S. Wu, B. Xu and C. Y. Ouyang, *Chin. Phys. B*, 2016, **25**, 018206.
- 55 Z. Cheng, M. Liu, S. Ganapathy, C. Li, Z. L. Li, X. Y. Zhang, P. He, H. S. Zhou and M. Wagemaker, *Joule*, 2020, **4**, 1311–1323.
- 56 Z. G. Xue, D. He and X. L. Xie, *J. Mater. Chem. A*, 2015, **3**, 19218–19253.
- 57 D. C. Zhang, X. J. Xu, X. Y. Huang, Z. C. Shi, Z. S. Wang, Z. B. Liu, R. Z. Hu, J. Liu and M. Zhu, *J. Mater. Chem. A*, 2020, **8**, 18043–18054.
- 58 S. F. Wen, Z. F. Sun, X. Y. Wu, S. H. Zhou, Q. Z. Yin, H. Y. Chen, J. H. Pan, Z. W. Zhang, Z. L. Zhuang, J. Y. Wan, W. D. Zhou, D.-L. Peng and Q. B. Zhang, *Adv. Funct. Mater.*, 2025, **35**, 2422147.
- 59 P. Bharathi and S.-F. Wang, *ACS Appl. Nano Mater.*, 2025, **8**, 16706–16716.
- 60 Y. Rong, Z. Y. Lu, C. Jin, Y. D. Xu, L. Peng, R. H. Shi, T. Y. Gu, C. Y. Lu and R. Z. Yang, *ACS Sustainable Chem. Eng.*, 2023, **11**, 785–795.
- 61 Y. H. Liang, N. Chen, F. Li and R. J. Chen, *ACS Appl. Mater. Interfaces*, 2022, **14**, 47822–47830.
- 62 L. He, J.-H. Cao, Y.-K. Wang and D.-Y. Wu, *Energy Adv.*, 2022, **1**, 1028–1034.
- 63 F. R. Ma, Y. X. Liu, X. R. Du and Q. Q. Lu, *Solid State Ionics*, 2024, **405**, 116450.
- 64 Y. C. Wu, M. Chao, C. Y. Lu, H. Y. Xu, K. Zeng, D. C. Li and R. Z. Yang, *J. Power Sources*, 2024, **599**, 234206.
- 65 S. Li, G. C. Sun, M. He and H. Li, *ACS Appl. Mater. Interfaces*, 2022, **14**, 20962–20971.
- 66 Q. Q. Zhou, C. Y. Li, B. Wang, W. W. Ding, J. J. Lu, B. F. Sheng, W. Li, W. J. Zhu, Q. Ni and X. Han, *J. Colloid Interface Sci.*, 2025, **690**, 137302.



- 67 J. T. Tang, L. D. Wang, C. H. Tian, T. Huang, J. J. Zhang, L. C. Zeng and A. S. Yu, *J. Alloys Compd.*, 2023, **960**, 170736.
- 68 D. Hu, G.-R. Zhu, P.-H. Duan, S.-C. Chen, G. Wu and Y.-Z. Wang, *Adv. Sci.*, 2025, **12**, 2501012.
- 69 L. G. Yi, X. Y. Chen, J. J. Huang, J. L. Liu, H. H. Hu, H. H. Zhao, T. J. Wu, L. Liu and X. Y. Wang, *J. Energy Storage*, 2025, **120**, 116459.
- 70 Y. L. Liu, Y. L. Xu, Y. Zhang, C. Yu and X. K. Sun, *J. Colloid Interface Sci.*, 2023, **644**, 53–63.
- 71 D. Z. Yang, Y. N. Yang, Y. Y. Sun and T. Zhang, *Adv. Funct. Mater.*, 2025, **35**, 2420202.
- 72 Ji.-H. Cao, P. Zhang, Y.-K. Wang and D.-Y. Wu, *Batteries Supercaps*, 2025, **8**, e202400463.
- 73 D. M. Reinoso, N. Ureña, M. T. Perez-Prior, B. Levenfeld and A. Varez, *Polymer*, 2024, **296**, 126728.
- 74 Y. K. Lin, K. Liu, M. C. Wu, C. Zhao and T. S. Zhao, *ACS Appl. Energy Mater.*, 2020, **3**, 5712–5721.
- 75 A. Mashekova, Y. Baltash, M. Yegamkulov, I. Trussov, Z. Bakenov and A. Mukanova, *RSC Adv.*, 2022, **12**, 29595–29601.
- 76 Y. Benabed, M. Rioux, S. Rousselot, G. Hautier and M. Dollé, *Front. Energy Res.*, 2021, **9**, 682008.
- 77 C. Yan, X.-B. Cheng, Y. Tian, X. Chen, X.-Q. Zhang, W.-J. Li, J.-Q. Huang and Q. Zhang, *Adv. Mater.*, 2018, **20**, 1707629.
- 78 F. Zheng, Z. P. Song, H. T. Li, Y.-Z. Zheng and X. Tao, *Electrochim. Acta*, 2022, **436**, 141395.
- 79 K.-W. Liu, P.-H. Hsu, J.-K. Chang, F.-M. Wang and W.-R. Liu, *Ceram. Int.*, 2025, **51**, 22556–22564.
- 80 Y. M. Jin, C. J. Liu, X. Zong, D. Li, M. Y. Fu, S. P. Tan, Y. P. Xiong and J. H. Wei, *J. Power Sources*, 2020, **460**, 228125.
- 81 S. Li, J. Z. Lu, Z. Geng, Y. Chen, X. Q. Yu, M. He and H. Li, *ACS Appl. Mater. Interfaces*, 2022, **14**, 1195–1202.
- 82 D. Li, L. Chen, T. S. Wang and L.-Z. Fan, *ACS Appl. Mater. Interfaces*, 2018, **10**, 7069–7078.
- 83 H. Choi, H. Kwon and H.-T. Kim, *ACS Appl. Energy Mater.*, 2023, **6**, 802–811.
- 84 M. Ghafari, Z. Sanaee, A. Babaei and S. Mohajerzadeh, *J. Power Sources*, 2025, **652**, 237608.
- 85 X. L. Xue, X. X. Zhang, Y. C. Liu, S. J. Chen, Y. Q. Chen, J. H. Lin and Y. N. Zhang, *Energy Technol.*, 2020, **8**, 2000444.
- 86 X. Q. Liu, S. Peng, S. Y. Gao, Y. C. Cao, Q. L. You, L. Y. Zhou, Y. C. Jin, Z. H. Liu and J. Y. Liu, *ACS Appl. Mater. Interfaces*, 2018, **10**, 15691–15696.
- 87 X. W. Yu, J. Y. Li and A. Manthiram, *ACS Mater. Lett.*, 2020, **2**, 317–324.
- 88 Z. Chen, G.-T. Kim, J.-K. Kim, M. Zarrabeitia, M. Kuenzel, H.-P. Liang, D. Geiger, U. Kaiser and S. Passerini, *Adv. Energy Mater.*, 2021, **11**, 2101339.
- 89 S. K. Choi, I. W. Cho, Y. Myung, S. Y. Cho, J. Choi and M. Yang, *ACS Appl. Energy Mater.*, 2025, **8**, 6222–6231.
- 90 Y. M. Jin, X. Zong, X. B. Zhang, Z. G. Jia, S. P. Tan and Y. P. Xiong, *J. Power Sources*, 2022, **530**, 231297.
- 91 S. H. Siyal, M. J. Li, H. Li, J.-L. Lan, Y. H. Yu and X. P. Yang, *Appl. Surf. Sci.*, 2019, **494**, 1119–1126.
- 92 G.-H. Dong, Y.-Q. Mao, G.-M. Yang, Y.-Q. Li, S.-F. Song, C.-H. Xu, P. Huang, Ni. Hu and S.-Y. Fu, *ACS Appl. Energy Mater.*, 2021, **4**, 4038–4049.
- 93 X. Z. Liu, X. T. Wang, F. Li, H. Y. Qiao, L. H. Jiang, Z. Y. Wan, Z. Wei and X. M. Liu, *Nano Res.*, 2025, **18**, 94907230.
- 94 X. Han, L. H. Gu, Z. F. Sun, M. F. Chen, Yi. G. Zhang, L. S. Luo, M. Xu, S. Y. Cen, H. D. Liu, J. Y. Wan, Y.-B. He, J. Z. Chen and Q. B. Zhang, *Energy Environ. Sci.*, 2023, **16**, 5395–5408.
- 95 S.-B. Hong, Y.-R. Jang, H. Kim, Y.-C. Jung, G. Shin, H. J. Hah, W. Cho, Y.-K. Sun and D.-W. Kim, *Adv. Energy Mater.*, 2024, **14**, 2400802.
- 96 A. Kızılbaşlan, R. Kızılbaşlan, A. Miura and K. Tadanaga, *Nano Today*, 2025, **60**, 102556.
- 97 X. Y. Bai, F. Xie, Z. Y. Zhang, M. L. Cao, Q. Wang, S. W. Wang, C. Y. Liu, X. Su, Z. Lin and G. L. Cui, *Adv. Energy Mater.*, 2024, **14**, 2401336.
- 98 L. Jia, J. H. Zhu, X. Zhang, B. J. Guo, Y. B. Du and X. D. Zhuang, *Electrochem. Energy Rev.*, 2024, **7**, 12.
- 99 J. X. Yuan, H. Dong, B. Wang, M. Qiu, Z. D. Liu, X. J. Wu, S. Zhong, G. S. Tong, Z. Y. Chen, J. C. Zhang, Q. Zhang, J. H. Zhu and X. D. Zhuang, *Chem. Eng. J.*, 2024, **487**, 150489.
- 100 Y. N. Zhang, J. M. Yu, H. S. Shi, S. H. Wang, Y. J. Lv, Y. Zhang, Q. Yuan, J. J. Liang, T. Y. Gao, R. Wei, X. Chen, L. Y. Wang, Y. Yu and W. Liu, *Adv. Funct. Mater.*, 2025, **35**, 2421054.
- 101 Y. D. Xu, M. Tian, Y. Rong, C. Y. Lu, Z. Y. Lu, R. H. Shi, T. Y. Gu, Q. Zhang, C. C. Jin and R. Z. Yang, *J. Colloid Interface Sci.*, 2023, **641**, 396–403.
- 102 D. Wang, F. Zheng, Z. P. Song, H. T. Li, Y. C. Yu and X. Tao, *Ind. Eng. Chem. Res.*, 2022, **61**, 14891–14897.
- 103 Z. Chen, Y. Wang, K. P. Zhu, Z. Q. Zhao, X.-A. Li, Y. X. Wu, X. W. Dou, M. H. Chen and C. Y. Ouyang, *Energy Environ. Mater.*, 2025, e70018.
- 104 W. M. Carvalho, L. Cassayre, D. Quaranta, F. Chauvet, R. El-Hage, T. Tzedakis and B. Biscans, *J. Energy Chem.*, 2021, **61**, 436–445.
- 105 B. Y. He, Y. Zhong, Z. W. Yan, T. Liu, X. Liu, Y. H. Du, Y. M. Yang, L. X. Yang, R. C. Zhang, Y. Q. Su, Z. Huang, B. Q. Xu and G. Zhang, *Adv. Funct. Mater.*, 2025, **35**, 2416779.
- 106 H. H. Liu, Y. B. Zhao, J. S. Zhou, P. Li, S.-H. Bo and S.-L. Chen, *ACS Appl. Energy Mater.*, 2019, **3**, 1260–1264.
- 107 J. Zhou, Y. Zhao, H. Liu, X. Tang, S.-L. Chen and S.-H. Bo, *J. Mater. Res.*, 2022, **37**, 3283–3296.
- 108 J. H. Hu, Z. T. Sun, Y. R. Gao, P. Li, Y. F. Wu, S. W. Chen, R. B. Wang, N. N. Li, W. G. Yang, Y. X. Shen and S.-H. Bo, *Cell Rep. Phys. Sci.*, 2022, **3**, 100938.
- 109 J. Tippens, J. C. Miers, A. Afshar, J. A. Lewis, F. J. Q. Cortes, H. Qiao, T. S. Marchese, C. V. Di Leo, C. Saldana and M. T. McDowell, *ACS Energy Lett.*, 2019, **4**, 1475–1483.



- 110 J. A. Lewis, F. J. Q. Cortes, Y. Liu, J. C. Miers, A. Verma, B. S. Vishnugopi, J. Tippens, D. Prakash, T. S. Marchese, S. Y. Han, C. Lee, P. P. Shetty, H. W. Lee, P. Shevchenko, F. De Carlo, C. Saldana, P. P. Mukherjee and M. T. McDowell, *Nat. Mater.*, 2021, **20**, 503–510.
- 111 F. Sun, C. Wang, M. Osenberg, K. Dong, S. Zhang, C. Yang, Y. Wang, A. Hilger, J. Zhang, S. Dong, H. Markotter, I. Manke and G. Cui, *Adv. Energy Mater.*, 2022, **12**, 2103714.
- 112 J. Li, J. J. Chen, X. S. Xu, J. Sun, B. L. Huang and T. S. Zhao, *Energy Environ. Sci.*, 2024, **17**, 5521–5531.
- 113 H. W. Gao, C. Lin, Y. P. Liu, J. S. Shi, B. W. Zhang, Z. F. Sun, Z. Li, Y. Wang, M. H. Yang, Y. Cheng and M.-S. Wang, *Sci. Adv.*, 2025, **11**, eadt4666.
- 114 A. Chen, N. Li, C. X. Sun, Y. M. Qin, L. Y. Qi, H. P. Zhang and H. F. Bao, *Chem. Eng. J.*, 2025, **520**, 166104.
- 115 X. X. Hao, K. Chen, Y. P. Tang, X. J. Zhong and K. F. Cai, *J. Alloys Compd.*, 2023, **942**, 169064.
- 116 B. Nie, T.-W. Wang, S. W. Lee and H. T. Sun, *ACS Appl. Mater. Interfaces*, 2024, **16**, 67635–67641.
- 117 J. Park, Y. Shim, J. H. Chang, S.-H. Kim, Y. K. Kang, J. W. Lee, D. S. Jung, J. M. Yuk, C.-W. Lee and J. Suk, *Chem. Eng. J.*, 2024, **496**, 153847.
- 118 S. N. He, Y. L. Xu, B. F. Zhang, X. F. Sun, Y. J. Chen and Y. L. Jin, *Chem. Eng. J.*, 2018, **345**, 483–491.
- 119 F. Wang, M. Zhang, Z. X. Fang, H. P. Zhou, J. T. Wu, Z. Q. Xu, N. X. Zhou, Y. H. Zhang, Z. Zeng and M. Q. Wu, *Energy Storage Mater.*, 2025, **77**, 104198.
- 120 M. Ghafari, Z. Sanaee, A. Babaei and S. Mohajezadeh, *J. Mater. Chem. A*, 2023, **11**, 7605–7616.
- 121 Z. T. Tu, K. Q. Chen, S. J. Liu and X. Wu, *Small Methods*, 2025, 2401912.
- 122 Y. T. Wang, X. Y. Zhang, X. W. Lang, Z. Li, C. Zhang, X. T. Feng and C. Shi, *Chem. Eng. J.*, 2025, **508**, 160824.
- 123 Z. R. Yao, K. J. Zhu, X. Li, J. Zhang, J. Li, J. Wang, K. Yan and J. S. Liu, *ACS Appl. Mater. Interfaces*, 2021, **13**, 11958–11967.
- 124 X. P. Yi, Y. Yang, J. J. Song, L. Y. Gan, B. T. Wang, G. L. Jiang, K. S. Xiao, X. N. Song, N. Wu, L. Q. Chen and H. Li, *Energy Storage Mater.*, 2025, **77**, 104191.
- 125 P. Baade and V. Wood, *iScience*, 2021, **24**, 102055.
- 126 H. T. Li, J. Liu, F. Deng, H. Lin, D. P. Wang and X. Tao, *J. Power Sources*, 2024, **602**, 234372.
- 127 Y. R. Gao, A. M. Nolan, P. Du, Y. F. Wu, C. Yang, Q. L. Chen, Y. F. Mo and S.-H. Bo, *Chem. Rev.*, 2020, **120**, 5954–6008.
- 128 S. Z. Xiong, X. Y. Xu, X. X. Jiao, Y. J. Wang, O. O. Kapitanova, Z. X. Song and Y. Y. Liu, *Adv. Energy Mater.*, 2023, **13**, 2203614.
- 129 Y. R. Gao, J. X. Huang, J. Cheng and S.-H. Bo, *Sci. China: Chem.*, 2023, **66**, 738–777.
- 130 M. A. Kraft, S. P. Culver, M. Calderon, F. Bocher, T. Krauskopf, A. Senyshyn, C. Dietrich, A. Zevalkink, J. Janek and W. G. Zeier, *J. Am. Chem. Soc.*, 2017, **139**, 10909–10918.
- 131 S. Muy, J. C. Bachman, L. Giordano, H.-H. Chang, D. L. Abernathy, D. Bansal, O. Delaire, S. Hori, R. Kanno, F. Maglia, S. Lupart, P. Lamp and Y. Shao-Horn, *Energy Environ. Sci.*, 2018, **11**, 850–859.
- 132 J. W. Abbott and F. Hanke, *J. Chem. Theory Comput.*, 2022, **18**, 925–934.
- 133 Z. F. Sun, Q. Z. Yin, H. Y. Chen, M. Li, S. H. Zhou, S. F. Wen, J. H. Pan, Q. Z. Zheng, B. Jiang, H. D. Liu, K. W. Kim, J. Li, X. Han, Y.-B. He, L. Zhang, M. C. Li and Q. B. Zhang, *Interdiscip. Mater.*, 2023, **2**, 635–663.
- 134 J. Li, M. S. Zhou, H.-H. Wu, L. F. Wang, J. Zhang, N. T. Wu, K. M. Pan, G. L. Liu, Y. G. Zhang, J. J. Han, X. M. Liu, X. Chen, J. Y. Wan and Q. B. Zhang, *Adv. Energy Mater.*, 2024, **14**, 2304480.

